SAND REPORT

SAND2002-8125
Unlimited Release
Printed January, 2002

Advanced Particle Control for Electric Discharge Light Systems

Mike Kanouff and Neal Fornaciari

Prepared by
Sandia National Laboratories
Albuquerque, New Mexico 87185 and Livermore, California 94550

Sandia is a multiprogram laboratory operated by Sandia Corporation, a Lockheed Martin Company, for the United States Department of Energy under Contract DE-AC04-94AL85000.

Issued by Sandia National Laboratories, operated for the United States Department of Energy by Sandia Corporation.

Available to DOE and DOE contractors from
U.S. Department of Energy
Office of Scientific and Technical Information
P.O. Box 62
Oak Ridge, TN 37831

Telephone: (865)576-8401
Facsimile: (865)576-5728
E-Mail: reports@adonis.osti.gov
Online ordering: http://www.doe.gov/bridge

Available to the public from
U.S. Department of Commerce
National Technical Information Service
5285 Port Royal Rd
Springfield, VA 22161

Telephone: (800)553-6847
Facsimile: (703)605-6900
E-Mail: orders@ntis.fedworld.gov
Online order: http://www.ntis.gov/ordering.htm

SAND2002-8125
Unlimited Release
Printed March 2002

Advanced Particle Control for Electric Discharge Light Systems

Mike Kanouff
Chemical and Materials Process Modeling
Sandia National Laboratories

Neal Fornaciari
Nanolithography
Sandia National Laboratories

ABSTRACT

We report on the results of an experimental and modeling study of a gas curtain mitigation system designed to prevent debris generated by a discharge light source from depositing on plasma-facing optics. The intent of the gas curtain is to entrain debris and deflect it away from sensitive optics. To facilitate the experimental portion of this study, a new laboratory was constructed that include two new roots-based vacuum pumps. This new experimental setup facilitated operation of the gas curtain at flow rates greater than ten times previously achievable while maintaining ten times lower pressure in the chamber. The experimental results showed a 100x reduction in particulate deposition rate and a 17x reduction in erosion with the gas curtain operational. The modeling results agreed quite well with the experimental measurements and will be used as a predictive tool for future design improvements.

Acknowledgements

The work described herein resulted from contributions by many different people. The authors would like to thank Ken Stewart and Steve Karim for their outstanding efforts in getting the hardware designed and built under tremendous time and budget pressure. Additionally, we would like to thank Dean Buchenauer and Howard Bender for their helpful insight. Finally, we would like to thank Jeff Chames and Nancy Yang for the SEM imaging and Miles Clift for his support performing Auger analysis.

Contents

Figures

1. Introduction

A difficulty inherent in using electric discharges to generate light is that the debris created by these sources tends to degrade the performance of the plasma-facing optics used to collect the light. There are a variety of applications for these light sources including x-ray lasers, soft x-ray microscopy, and advanced lithography. In the case of advanced lithography, for example, one of the most significant issues impeding commercial implementation is the lack of short-wavelength sources that can generate the necessary amount of power while maintaining an acceptable cost of ownership. Of the advanced source options available, plasma discharge sources, which generate short-wavelength light by means of direct conversion of electrical to actinic energy, have the lowest projected cost of ownership. This projection assumes, however, an essentially debris-free source that would support condenser optic lifetimes of 10^{11} pulses or about one year of continuous operation. Currently, the best of these discharge sources is several orders of magnitude short of that goal. The contamination generated by these sources tends to degrade the reflectivity of multilayer optics used in advanced lithography systems at such a rate that the use of these sources is not yet economically feasible. Material and design improvements intended to reduce debris generation have been incorporated, but these improvements alone will not be able to reduce the debris generation sufficiently. We report on the results of an experimental study of a gas curtain debris mitigation technique.

The gas curtain is designed to alter the trajectory of the debris enough to deflect it away from deposition on plasma-facing optics. The debris is thought to be small (less than one micron) and have large velocities (greater than 100 m/s) [Ref. 1]. The vacuum environment required to minimize absorption of the short wavelength light these sources generate will cause spreading of the gas curtain which will reduce its effectiveness. This spreading can be partially offset by expanding the gas in a diverging nozzle to establish a supersonic directed flow. The jet spreading will decrease with increasing Mach number at the exit of the nozzle.

The use of a gas curtain will increase the gas pressure in the vacuum system, which raises some concern regarding light absorption. The fraction of light absorbed, f_a, by a gas is described by Equation 1,

$$f_a = 1 - \exp(-n\mu_a s), \tag{1}$$

which shows that light absorption increases with the gas number density, n (or gas pressure), the absorption cross section, μ_a, and the light path length, s. The absorption cross section depends greatly on the chemical species. Helium is a good candidate gas because it has a small absorption cross section and it is an inert gas. The path length can be as large as 2 meters so the pressure in the chamber must be kept as low as possible.

In order to maintain low pressures in a vacuum chamber that contains a gas curtain a combination of strategies can be used. First, the curtain gas flow rate can be set to the minimum value that adequately deflects the particles. Second, additional vacuum pumps can be installed on the chamber. Third, a diffuser can be used that acts to capture the curtain gas while it is still at a relatively high pressure such that the captured gas can be efficiently pumped out of the chamber.

Figure 1 shows a sketch of a simple gas curtain design studied here for deflecting particulate debris generated by a capillary discharge light source. Gas (e.g. helium) flows from a high pressure source into the nozzle where it expands to supersonic velocities. The gas then exits the nozzle and flows laterally in front of the capillary discharge device, the source of the particles. Some of this gas enters the diffuser and is removed by a vacuum pump. The remainder of the gas flows into the chamber and is removed by a second vacuum pump. As a particle moves out from its point of origin toward the collection optic, it enters the supersonic gas flow field. The particle is deflected from the path it would have otherwise taken and moves harmlessly away from the optic.

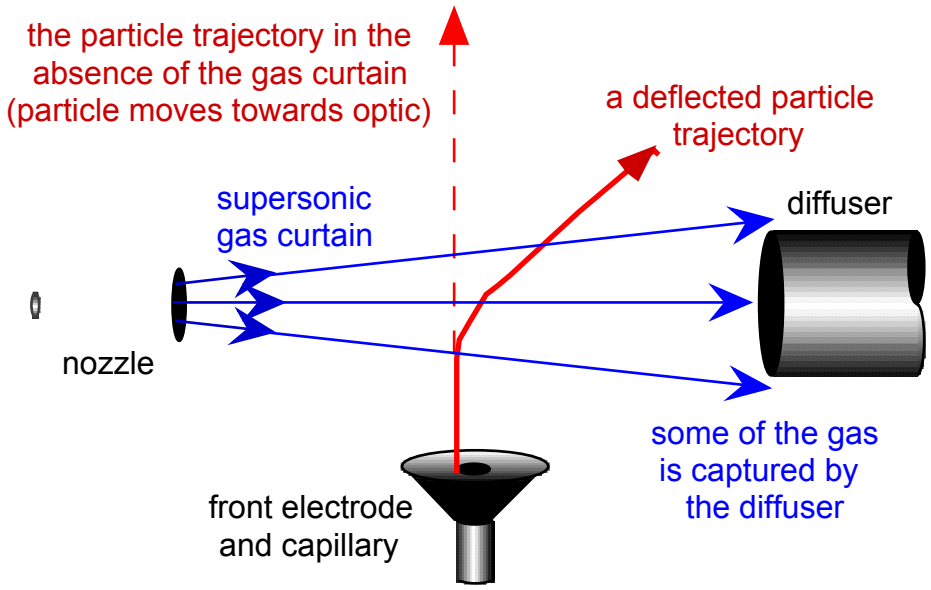

Figure 1. A schematic of the gas curtain conceptual design.

2. Theory

The gas curtain flow rate must be high enough to deflect particles and yet not so high as to result in excessive chamber pressures. The effect of the gas curtain design parameters on particle deflection and gas flow rate are discussed here based on simple gas dynamic theory where the expansion of the gas is assumed to be isentropic (inviscid and adiabatic). This theory will help explain the results obtained from the experiments and calculations.

Equation 2 describes the flow rate through a nozzle in the form of the throughput, Q, which is the form often used to describe the performance of vacuum pumps (independent of gas species) and is given by the product of the volumetric flow rate and the gas pressure. Equation 2 shows that Q increases with the gas source pressure, p_o (i.e. stagnation pressure), the nozzle throat area, A_{th}, and with decreasing molecular weight of the gas, W. This latter effect is due to the inverse relationship between the gas sound speed and W, i.e. the gas sound speed (and consequently the through put) decreases with increasing W. The ratio of specific heats, γ, in Equation 2 has a value of 5/3 for monatomic gases, which includes both helium and argon.

$$Q = A_{th} p_0 \left(\frac{\gamma + 1}{2} \right)^{\frac{1+\gamma}{2-2\gamma}} \sqrt{\frac{\gamma R T_0}{W}} \tag{2}$$

A gas curtain deflects particles through the action of a drag force. The drag force required to deflect a particle a given amount increases with both the particle mass and the particle velocity. The drag force on a particle is typically expressed in terms of a drag coefficient as,

$$F_D = C_D A_C \rho V_r^2 / 2 \tag{3}$$

where F_D is the drag force, C_D is the drag coefficient, A_C is the cross sectional area of the particle ($A_C = \pi r^2$ for a spherical particle), ρ is the local gas density and V_r is the relative velocity between the particle and the gas. The conditions in the gas curtain considered here include a high mach number and a large particle Knudsen number (equal to the ratio of the molecular mean free path to the particle diameter). For these conditions C_D is close to a constant value of approximately 2. Also, the gas velocity is typically large compared to the particle velocity so V_r may be approximated as just the gas velocity, V. The drag force then becomes proportional to the gas momentum flux, ρV^2, which is given by Equation 4, where Ma is the local gas Mach number. For all else being equal, Ma is independent of the gas species (assuming monatomic gases). Equation 4 shows that the gas momentum flux increases with p_0 and is independent of the gas species (i.e. W).

$$F_D \propto \rho V^2 = \gamma p_0 Ma^2 \left(1 + \frac{\gamma - 1}{2} Ma^2 \right)^{\frac{\gamma}{1-\gamma}} \tag{4}$$

Thus, the particle drag force required to deflect the particles determines the required value of p_0. For a given value of p_0, the gas flow rate will be larger for helium than for argon, so choosing argon will help ease the vacuum pumping requirement. However, if the vacuum pumping requirement can be easily met, helium should be chosen because it has a smaller absorption cross section.

It can be shown using some of the approximations discussed above that:

$$\tan(\theta) = \frac{3 C_D w \rho V^2}{4 \rho_p V_p^2 D_p} \tag{5}$$

where θ is the particle deflection angle, w is the width of the gas curtain, ρ_p is the particle density, V_p is the initial particle velocity and D_p is the particle diameter. This equation shows that the deflection angle will decrease with the particle density, the particle diameter and the square of the particle speed.

3. Experiment Description

Figure 2 shows a schematic of a vacuum chamber that houses a capillary discharge device, a gas nozzle, and a diffuser. Two nozzles were used, where both had conical shapes, a small nozzle with a throat (inlet) diameter of 0.308 mm and a exit diameter of 1.2 mm, and a large nozzle with a throat diameter of 0.600 mm and a exit diameter of 2.4 mm. The diffuser was located one inch from the nozzle exit where it was coaxial with the nozzle and is one inch in diameter. Helium was used to form the curtain in order to minimize absorption losses. Two large vacuum pump systems were used, an Aerzon V2000 roots blower system was connected to the diffuser, and an Aerzon HV9000 roots blower system was connected directly to the chamber. Pressure gauges were installed at various locations including at the inlet to the gas nozzle, in the diffuser, and in the chamber. A flow meter was used to measure the total flow rate through the nozzle.

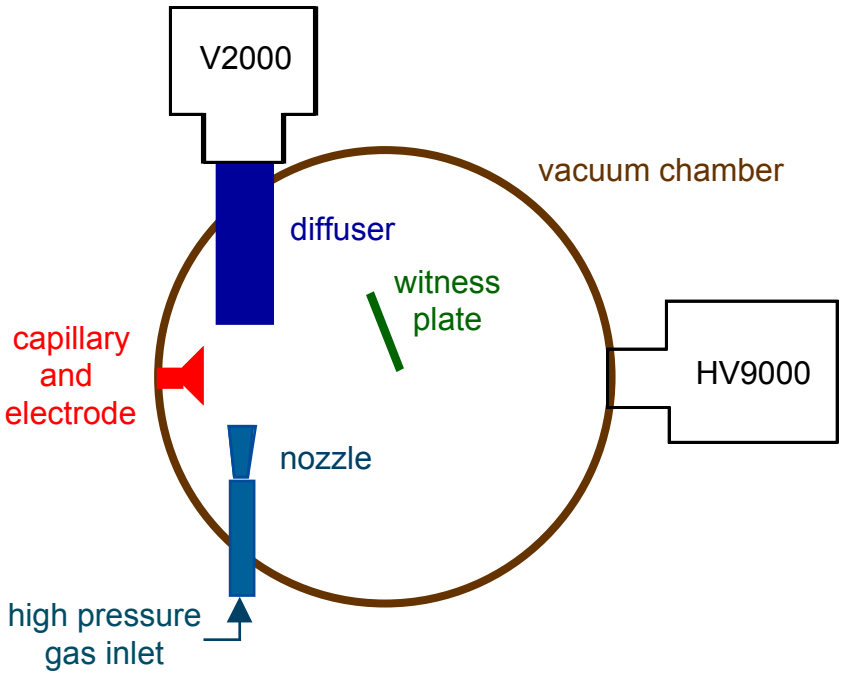

Figure 2. A schematic of the experimental apparatus.

3.1 Diffuser efficiency measurements

Measurements of the pump inlet pressures were used along with the pump performance curves to determine the amounts of gas entering the diffuser and the chamber. Separate runs were made where only one pumping system was used at a time in order to generate the pump performance curves. Helium flow rates up to approximately 1000 torr l/s were used.

3.2 Debris mitigation experiments

Experiments were carried out to measure the effectiveness of the gas curtain for deflecting particles. A witness plate was used to collect particles on the opposite side of the curtain from the lamp. Two experiment runs were carried out; in the first run, the witness plate was exposed to the discharge source without the use of a gas curtain, and in the second run a helium gas curtain

was used with a flow rate of 760 torr l/s. In each test, 1 million pulses of the capillary discharge device was used to generate particles. A clean witness plate was used for each test. A video camera (super VHS) was used to record images of trajectories of some of the larger particles generated by the lamp.

4. Experimental Results

4.1 Pump performance curves

The results for the pump performance curves, determined by experiment, are shown in Figure 3 and Figure 4 for the V2000 and HV9000 systems, respectively, in terms of the pumping speed as a function of pump inlet pressure. The results are compared to the performance estimates provided by the Hull Corporation, the pump vendor. The performance of the V2000 is close to that reported by Hull.

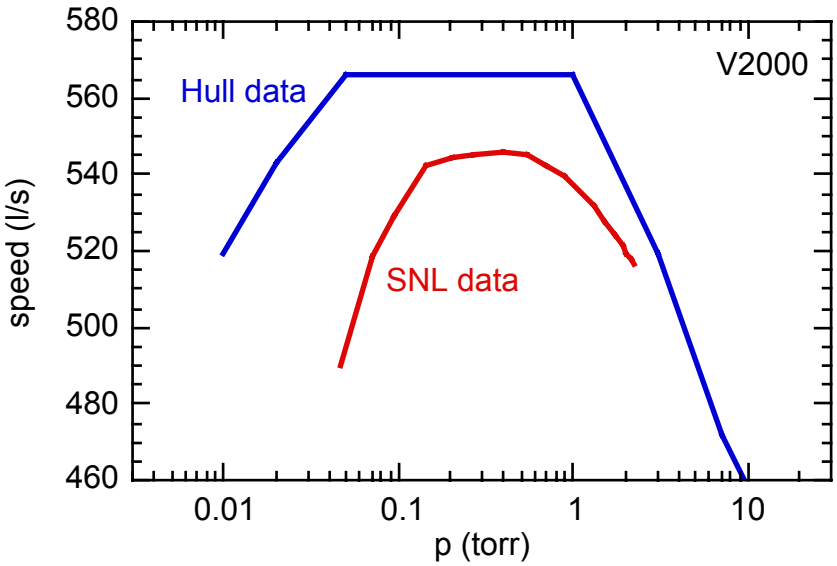

Figure 3. The experimentally determined pump performance curve for the V2000 (diffuser) system.

The performance of the HV9000 system is compared to two curves provided by Hull, one for air and another for helium. The measured performance lies between these two curves. Note that the measurements for the V2000 system spanned a range of pressures from 0.05 torr to 2 torr, while the range of pressures spanned by the measurements for the HV9000 system was 0.01 torr to 0.1 torr. The high pressure range was used for the V2000 because the diffuser is expected to capture the gas in the curtain while it is still at high pressure. The lower pressures used for the HV9000 spans the maximum range that would be acceptable in terms of EUV absorption losses in helium. Also, the HV9000 system has a much larger pumping speed than the V2000 system. The larger pumping speed is needed for the chamber because the pressures there must be maintained to much lower values than those in the diffuser.

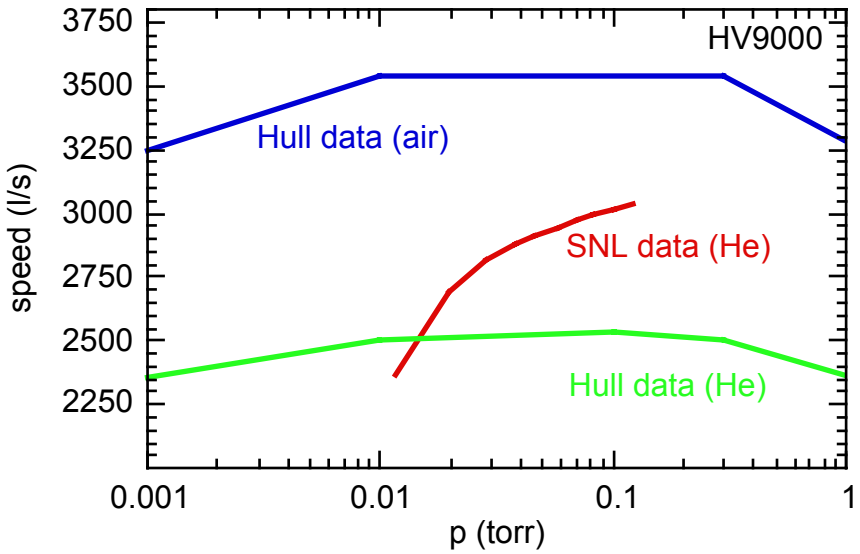

Figure 4. The experimentally determined pump performance curve for the HV9000 (chamber) system.

4.2 Diffuser efficiency

Figure 5 shows the measured pressures in the diffuser and chamber for the experiment run with the small nozzle. The diffuser pressure is much higher than that in the chamber. This makes it possible to pump out much of the gas at a relatively high pressure using the V2000 system. The chamber pressure was kept to a low value, well within the acceptable range in terms of EUV absorption losses. Data such as that shown in Figure 5 was used to determine the diffuser efficiency, as discussed below.

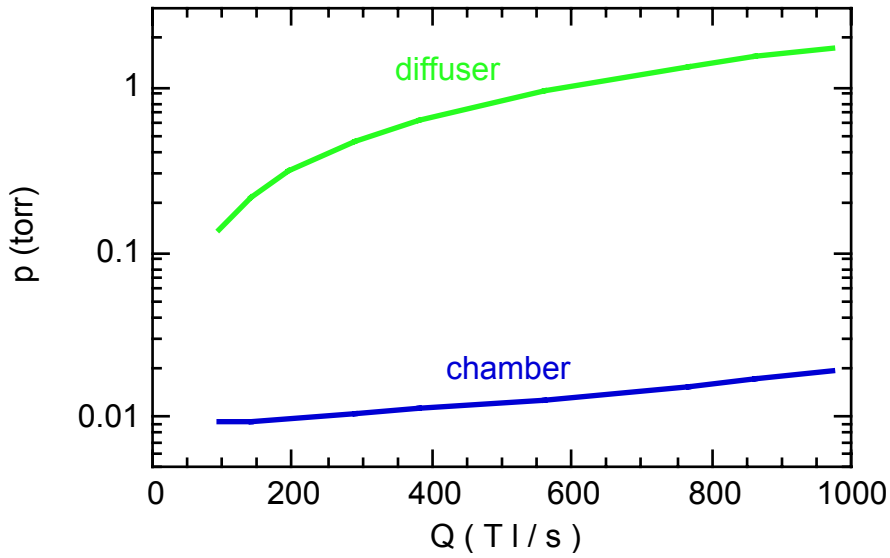

Figure 5. The measured pressures in the diffuser and chamber for the small nozzle as a function of He flow rate.

Figure 6 shows the diffuser efficiencies as a function of the total gas flow rate in the curtain for the small and large nozzles. The diffuser efficiency is defined as the ratio of the gas flow rate captured by the diffuser over the total gas flow rate in the curtain. Calculated results for the efficiency of the small nozzle are also shown for comparison, where the measured diffuser and chamber pressures were used as boundary conditions for the calculations. The measured efficiency for the small nozzle increases to near 95%, and then begins to decrease for flow rates exceeding 800 torr-liter/second. The calculated results for the small nozzle compare well with the measured results, although the calculated results decrease more rapidly for Q > 800 than the measured results. The measured efficiencies for the large nozzle are also large, although not as large as those for the small nozzle, and the efficiency for the large nozzle begins to decrease for Q > 400.

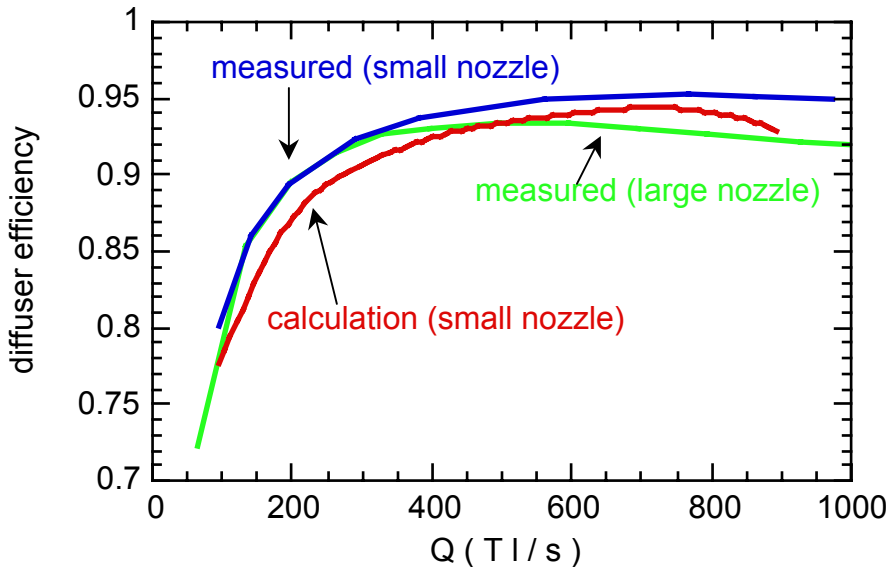

Figure 6. The measured and calculated diffuser efficiencies.

The experimentally determined diffuser efficiencies made use of the measured pump performance curves and the pump inlet pressures to determine the amount of gas entering each pumping system. As a check for the accuracy of this method, the sum of the flows entering the pumping systems was compared to the known total gas flow rate in the curtain, where the sum and the total should be equal. Figure 7 shows that the sum (of the gas flow entering the HV9000 and V2000 pump systems) was within ±4% of the total for all flow rates considered.

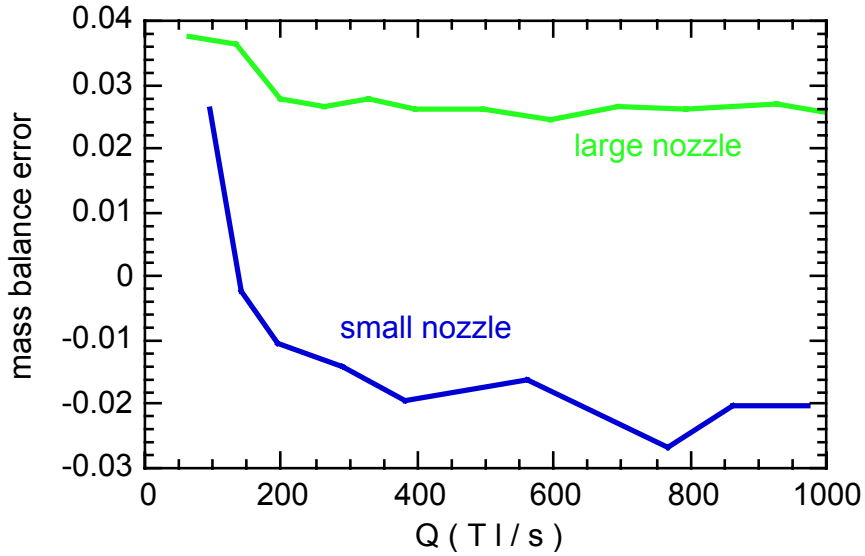

Figure 7. The mass balance error between the sum of the flows entering the pumping systems and the known total flow in the curtain, i.e. error = (sum-total)/total.

Although the difference between the diffuser efficiencies measured for the small and large nozzles appears small, this difference has a large effect on chamber pressure. This is because most of the gas enters the diffuser, and a small difference in the amount of gas entering the diffuser results in a large difference in the amount of gas entering the chamber. That is, for a flow rate of Q = 800 Tl/s, the diffuser efficiency for the small nozzle was 95% while it was 92% for the large nozzle. This means that 5% of the gas entered the chamber for the small nozzle while 8% of the gas entered the chamber for the large nozzle. Figure 8 shows that the chamber pressure for the large nozzle case was much larger than that for the small nozzle case. Consequently, the maximum flow rate used in the curtain must be limited to a lower value for the large nozzle in order to get the same chamber pressure and light absorption losses as with the small nozzle.

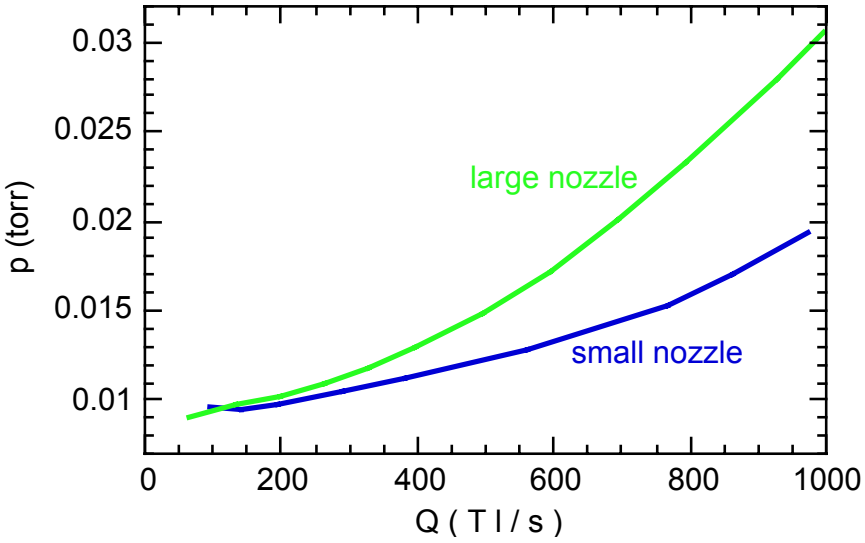

Figure 8. The measured chamber pressure for the small and large nozzle experiments.

4.3 Debris mitigation measurements

The mitigation efficiency of the gas curtain was determined by analysis of witness plates exposed to 1 million pulses both with and without the gas curtain operating. The witness plates were 1 cm square silicon substrates coated with 20 Mo/Si layer pairs and located 14 cm from the source (see Figure 2 for location). The source was operated at 500 Hz, 1500 V, and ~5 Torr xenon pressure with a 1 μs pulse width yielding a peak current of about 3.5 kA. The lamp was outfitted with 80/20 W/Cu electrodes.

4.3.1 Atomic debris mitigation

An analysis of the witness plates using Auger depth profiling reveals the amount of vapor debris that is deposited during an exposure run. For both cases the multilayer was sputtered through to the silicon substrate to determine how much erosion had occurred during the exposure. Figure 9 is a plot of the depth profile for the case without the gas curtain. The most significant result here is that only 3 of the original 20 layer pairs remain after 1 million pulses. Because of the significant amount of erosion that took place, no conclusion can be drawn regarding the rate of vapor deposition on the witness plate without the gas curtain. By contrast, Figure 10 reveals that only the silicon capping layer and perhaps part of first molybdenum layer were eroded when the gas curtain was operating. Figure 11 shows the composition near the surface of the witness plate from Figure 10. This plot shows a moderate amount of both tungsten and copper deposited on the surface of the witness plate with the gas curtain running. While at first glance this would seem to imply that the gas curtain is not working to deflect the vapor debris, a look at the geometry of the experimental setup reveals a more plausible explanation.

Figure 12 is a side-view of the gas curtain geometry. Part A shows the exclusion zone where debris generated by the lamp heading toward the witness plate would be intercepted by the gas curtain jet. Any debris generated and traveling within this exclusion zone would be deflected away from the witness plate. Part B highlights a zone where debris generated from the front electrode could circumvent the jet and be deposited on the witness plate. We believe that the tungsten and copper seen in Figure 11 are deposited via this mechanism.

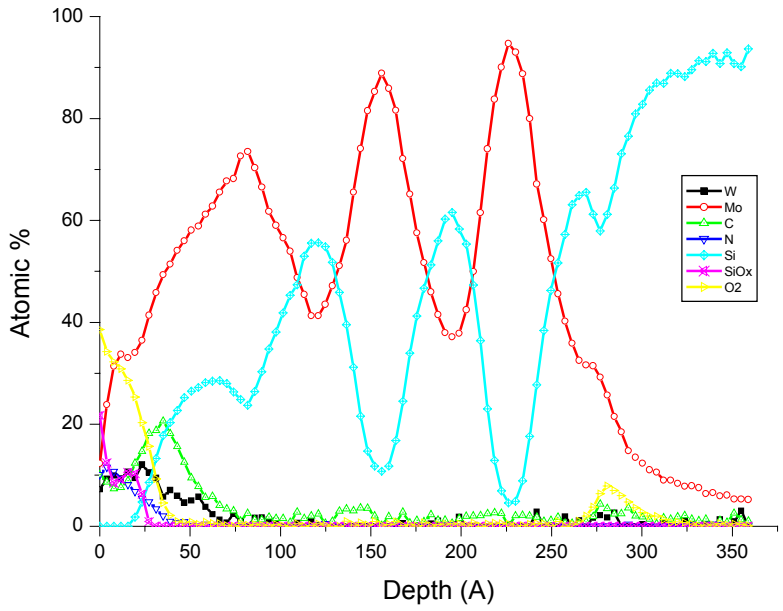

Figure 9. Auger depth profile of witness plate exposed without gas curtain

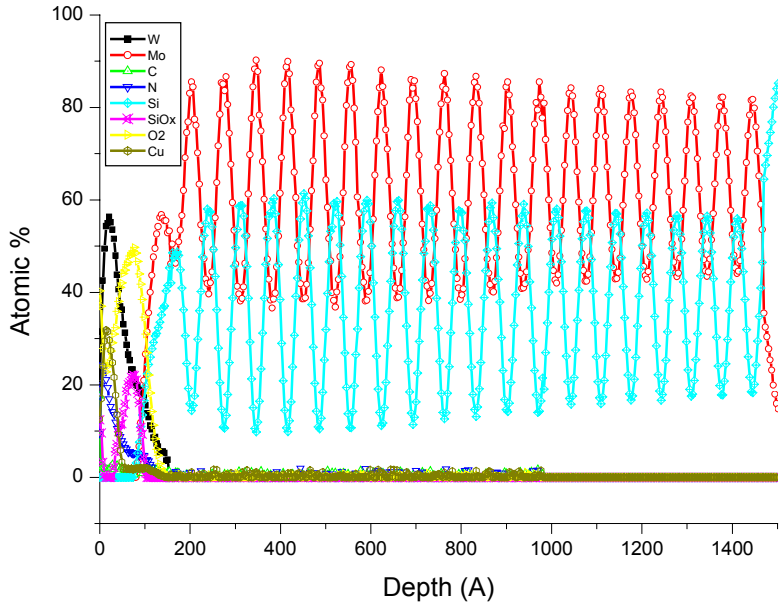

Figure 10. Auger depth profile of witness plate exposed with gas curtain.

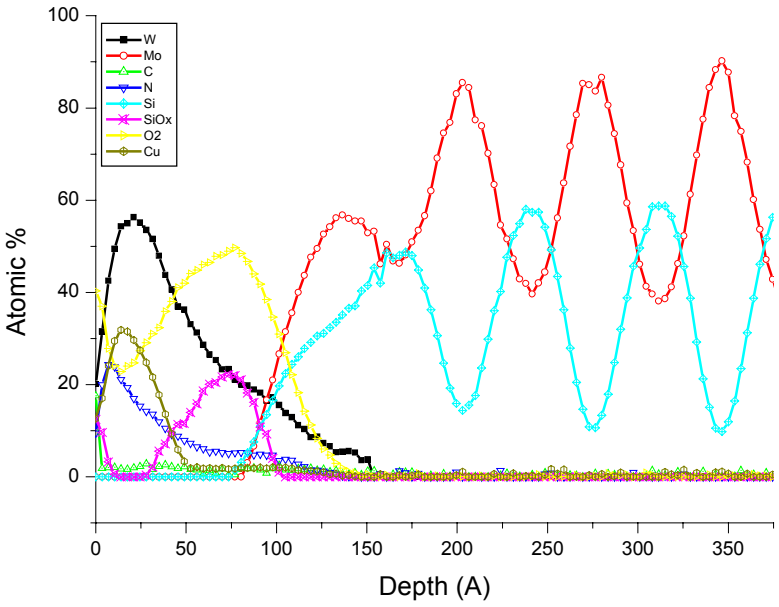

Figure 11. Blown-up plot near the surface of Figure 10.

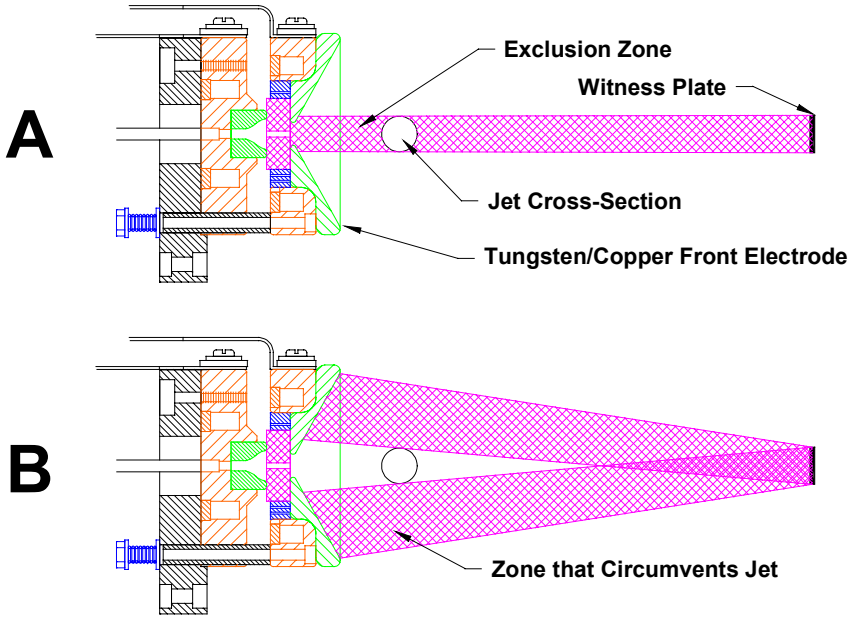

Figure 12. A shows the exclusion zone where the gas curtain jet intercepts debris generated at the lamp heading toward the witness plate. B shows the zone where debris generated at the front electrode can circumvent the jet and deposit on the witness plate.

4.3.2 Particulate debris mitigation

Some of the particles ejected from the lamp were sufficiently large to see without magnification. These particles glowed (i.e. self illuminated) apparently due to their high temperature. Video images of these particles appeared as streaks due to their high velocity. Figure 13 shows the trajectory of a particle exiting the lamp and entering the gas curtain. Upon entering the curtain, the particle is deflected nearly 90° toward the diffuser. Deflection angles this large are more than sufficient to protect the sensitive optics that would be used to collect light generated by the lamp. Many particles were observed in the video recording being deflected by similar angles. However, many other particles were deflected by much smaller angles. Some of these smaller deflection angles occurred for particles that entered the outer fringes of the gas curtain, but it is not clear if this was the case for all of the smaller deflection angles observed in the video recording. Other portions of the video recording (not shown here) showed that there was a large range of initial trajectory angles for the particles. In one particular instance, a particle was observed to strike the outer housing of the nozzle and to bounce off after breaking up into two pieces.

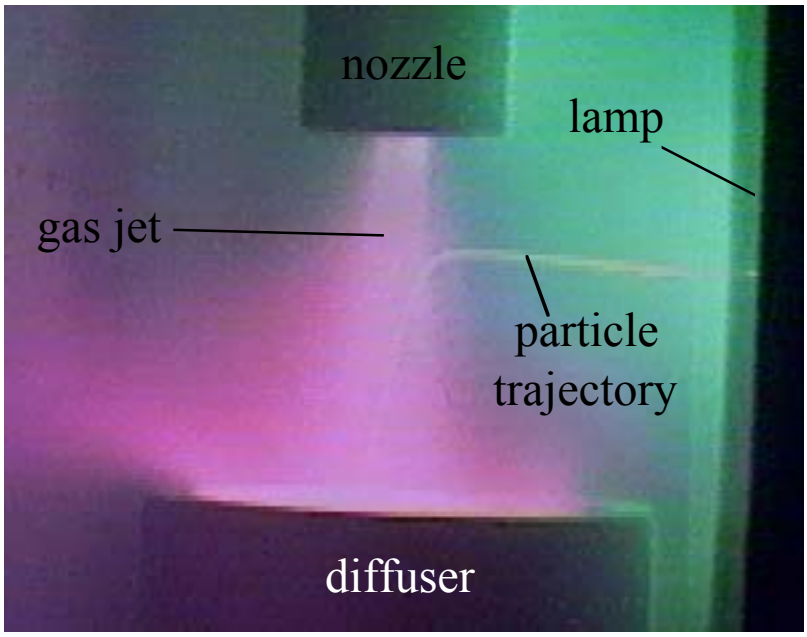

Figure 13. A video image of the gas curtain deflecting a particle into the diffuser.

The witness plates from the debris tests were examined to determine the effectiveness of the curtain for deflecting debris away from the plate. A scanning electron microscope (SEM) was used to image portions of the plates at 1000X and 2500X magnifications. Figure 14 shows 1000X images of the plates from the tests with and without the curtain. Particles appear white in the images while the bare portions of the witness plate appear dark gray. The figure shows that many particles were deposited on the witness plate from the test without the curtain (left image), while only a few particles were deposited on the plate from the test with the curtain (right image). Figure 15 shows the 2500X images, and again it can be seen that many more particles were deposited on the plate from the 'no curtain' test than on that from the 'curtain' test. The 2500X images reveal more of the smaller particles that cannot be seen in the 1000X images.

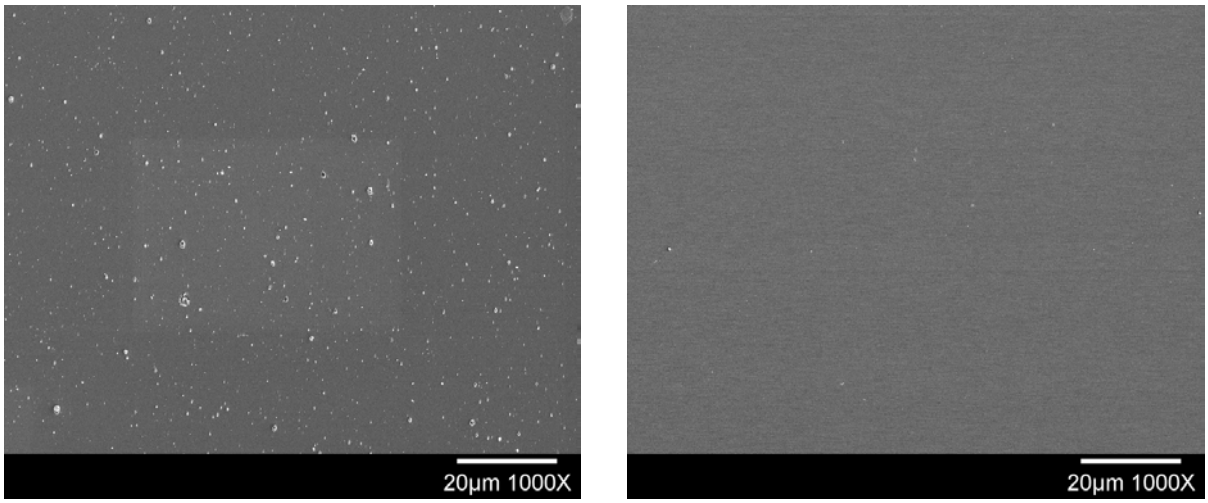

Figure 14 SEM images with 1000X magnification of portions of the witness plates used in the 'no curtain' (left) and 'curtain' (right) experiments

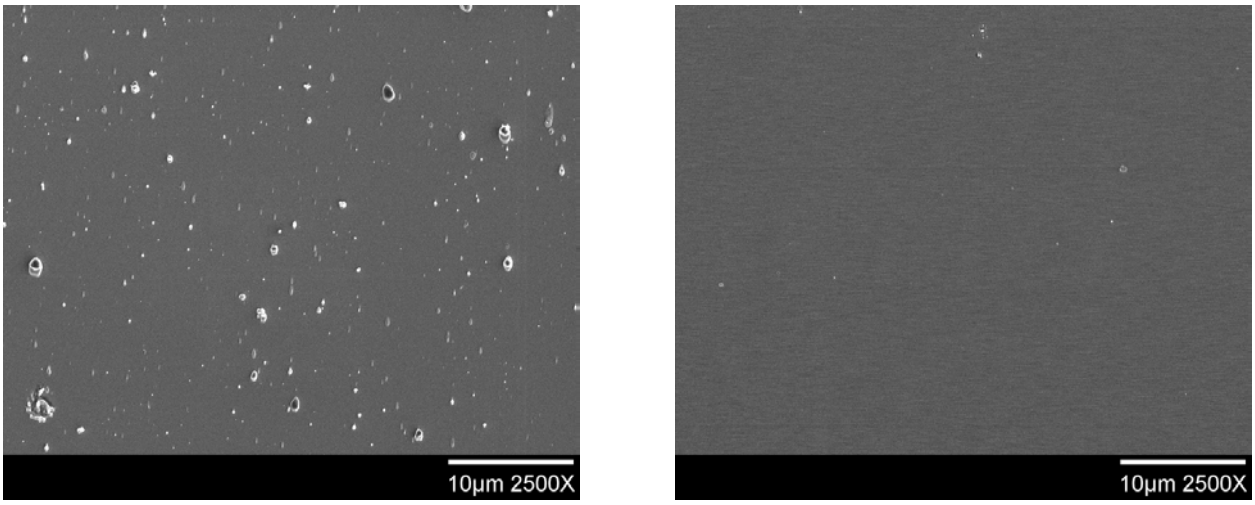

Figure 15. SEM images with 2500X magnification of portions of the witness plates used in the 'no curtain' (left) and 'curtain' (right) experiments.

The SEM images shown in Figure 15 were converted to a binary format (i.e. black and white) in order to contrast the particles from the bare plate surface. A threshold must be chosen to separate white (particles) from black (plate). Since the choice of threshold is somewhat subjective, a range of values was used to determine the sensitivity to the choice of threshold. Figure 16 shows the results of this sensivity study, including the result for an image taken from an unexposed (blank) witness plate that had no visible particles on it. The figure shows the fraction of each image that is white, i.e. the fraction of the image that is occupied by particles. The particle fraction decreases with increasing threshold because for small values of the threshold a large portion of the bare plate is converted to white while for large thresholds many of the particle converted to black. Even the result for the blank plate shows a non-zero particle fraction for small thresholds, although it rapidly decreases to low values with increasing threshold. The results show that the particle fraction on the 'no curtain' witness plate was approximately 1%, and that the particle fraction on the 'curtain' witness plate was near 0.01%.

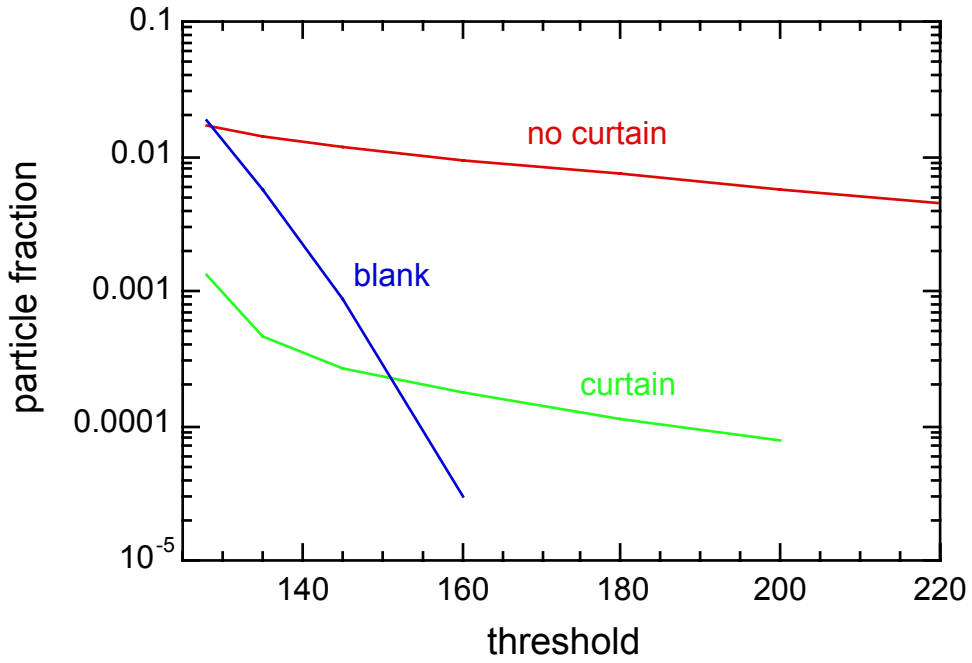

Figure 16. The results of an image analysis for the particle fraction in the SEM images of the witness plates from the 'curtain' test, 'no curtain' test, and a blank plate.

After converting the SEM images to a binary format, the particle size distribution was determined. Figure 17 shows this size distribution in a histogram format, i.e. particle sizes were grouped into finite sized bins and the number of particles falling into each bin are shown. The results show that the particle sizes range from 0.05 to almost 1 micron, the number of particles decreases with increasing particle size, and the gas curtain appears to have deflected all of the larger particles.

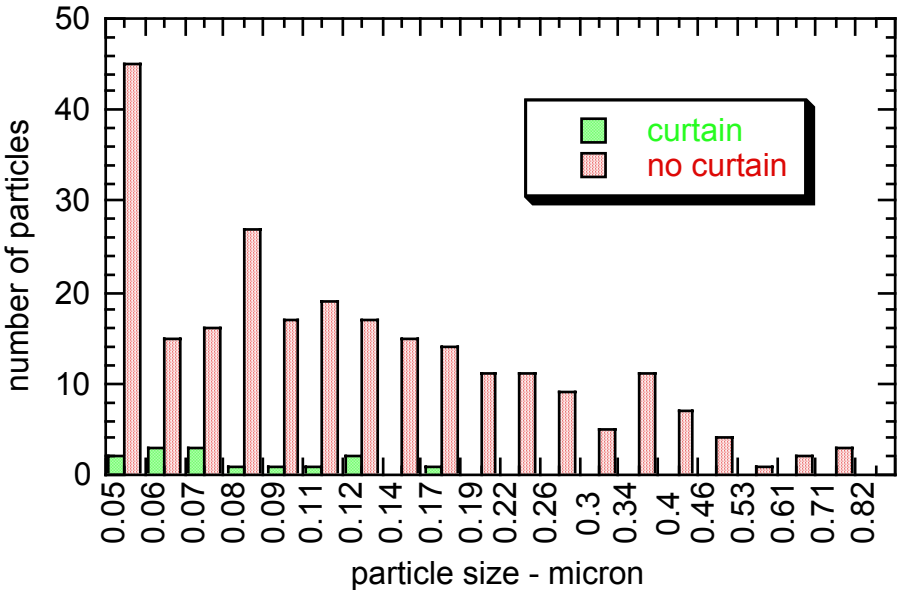

Figure 17. A histogram of the particle sizes on the witness plates from the 'curtain' and 'no curtain' cases.

The use of the gas curtain resulted in a reduction in the number particles on the witness plate by a factor of approximately 100. While this is a significant reduction, it may not be sufficient to protect the optics in a commercial EUV lithography tool for the duration required to make the tool economically acceptable. In order to improve the protection that the curtain provides, the path that the particles took to the 'curtain' witness plate must be determined.

One possibility is that these particles went directly through the curtain. This would require that they travel at a significantly higher speed than the particle seen in Figure 13 to maintain a near straight trajectory as they travel through the curtain and to make up for their much smaller size (all of the particles on the 'curtain' witness plate were noted to be relatively small as shown in Figure 17).

It may be that the particles seen on the 'curtain' witness plate did not take a direct path through the curtain. Instead, their initial path may have been away from the curtain (and witness plate) followed by an impact on a hardware surface somewhere in the chamber where they bounced and were re-directed toward the witness plate. Evidence of particles bouncing upon impact with a solid surface was seen in the video recording of the experiments. Or, the particles on the 'curtain' witness plate are small enough that they could have been suspended in the 0.022 torr gas in the chamber and were transported to the witness plate via the circulating flows that are likely to exist in the chamber during operation of the curtain.

5. Modeling

5.1 Description

The Sandia general purpose compressible fluid mechanics code, SACARRA, was used to calculate the gas flow fields. This code solves the general form of the Navier-Stokes equations, i.e. the gas is assumed to be a continuum viscous fluid. This is a valid assumption for the flow field near to the nozzle and diffuser for the relatively high gas source pressures considered here. All gas flow fields were assumed to be axisymmetric. The model included the nozzle, a portion of the gas feed tube upstream of the nozzle, the diffuser and a portion of the vacuum chamber. Experimentally obtained values for the pressures in the diffuser and chamber were used as boundary conditions for the calculations.

The calculated results for the gas density and velocity fields were used to calculate particle trajectories in the curtain. Aerodynamic drag, F_D, was assumed to be the only force acting on the particles, and the particles were assumed to be spheres. F_D is a vector with a direction opposite to that of particle-gas relative velocity, V_r. A comprehensive drag coefficient [$C_D \equiv 2F_D/(A_C \rho V_r^2)$] correlation by Henderson [Ref. 2] was used that is valid for a wide range of flow conditions including subsonic, supersonic, continuum and free molecular. Given the local gas state and velocity and the particle velocity, the drag force can be evaluated. Newton's second law, $F_D = m_p dV_p/dt$, was solved for the change in particle (absolute) velocity, V_p, where m_p is the particle mass. In this equation F_D and V_p are vectors and the change in V_p (i.e. dV_p) is in the same direction as F_D. The calculated particle trajectories presented here all assume that the particles were made of tantalum based on energy dispersive spectrum analysis of particles seen on witness plates. Tantalum is one of the materials used in the discharge lamp.

5.2 Calculated results for the gas flow field

Calculations for the diffuser efficiency and particle trajectories were carried out for comparison to the experimental results. Experimental validation of the model provides the basis for using it with confidence to study advanced gas curtain designs. Some of this validation was established above (see Figure 6) in the comparison of measured and calculated diffuser efficiencies. The first step towards calculating diffuser efficiencies and particle trajectories is to calculate the gas flow field in the curtain. Results for the flow and pressure fields are shown in Figure 18 for a helium flow rate of 760 Tl/s, the value used in the experiments. The streamlines indicate that some of the gas in the outer periphery of the curtain flows around the diffuser, but most of it is captured by the diffuser. There is a conical shaped shock wave located inside the diffuser that results in a sudden increase in pressure as the flow crosses it. This shock wave also results in a sudden turn of the gas flow towards the axis of symmetry. The 'high' pressure in the diffuser is beneficial because it reduces the volume of the gas flowing into the vacuum pump attached to the diffuser making it easier for the pump to evacuate it.

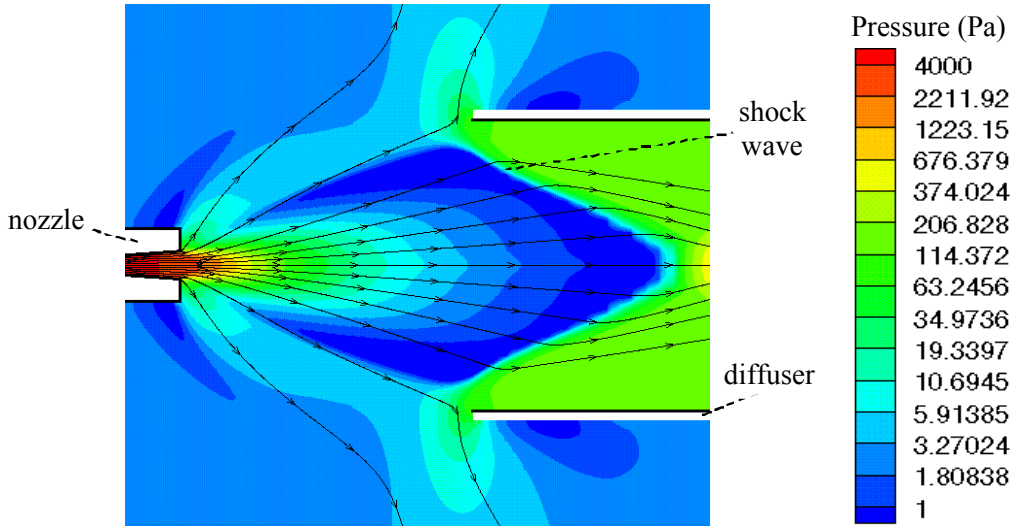

Figure 18. Calculated results for the flow and pressure fields in the helium gas curtain for a flow rate of 760 Tl/s.

Figure 19 shows the calculated density field in the curtain. The density is a maximum at the nozzle exit and it decreases rapidly with distance from the nozzle. The gas density is large in the space between the nozzle and diffuser and in the diffuser relative to that in the surrounding region where it is approximately equal to that which would exist in the remainder of the chamber. Thus, a local region of high velocity gas with large density can be established in otherwise medium vacuum conditions. This is essential to the success of the gas curtain for this application where the small region of dense, high velocity gas is needed to deflect particles while elsewhere the density must be kept small in order to minimize EUV light losses due to absorption by the gas.

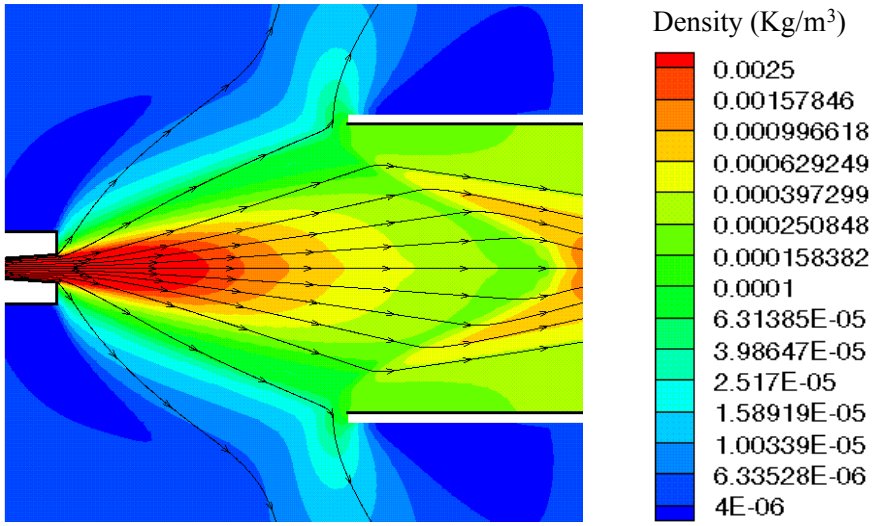

Figure 19. Calculated results for the flow and density fields in the helium gas curtain for a flow rate of 760 Tl/s.

The calculated results for the gas density field were used to calculate the EUV transmission through the gas curtain. Figure 20a shows the transmission through the center of the curtain perpendicular to its axis, starting at a point 2.54 cm from the axis. The transmission remains near unity until the curtain axis (y = 0) is approached, where the transmission rapidly decreases over a 1 cm distance to a value near 0.88 at a point on the far side of the curtain axis. From there the transmission will continue to decrease at a very slow rate due to the low density gas that exists in the vacuum chamber. Assuming a 2 meter total path length for the EUV in the vacuum chamber, there would be a subsequent loss of EUV (i.e. outside of the curtain) of 7%. Thus, the total loss of EUV light is composed of two contributions; 1) that due to the high density gas in the curtain, and 2) that due to the long path length in the low density gas filling the remainder of the vacuum chamber. The total transmission for a path going through the center of the curtain would be 0.88 $\times$ 0.93 = 0.82. Figure 20b shows the total curtain transmission through the gas curtain (i.e. through a 5 cm wide region surrounding the curtain) as a function of the distance along the curtain axis. The results show that the transmission is small near the nozzle exit (x = 0). The study of advanced gas curtain designs should include consideration of keeping the near-nozzle-exit region out of the path of the EUV light.

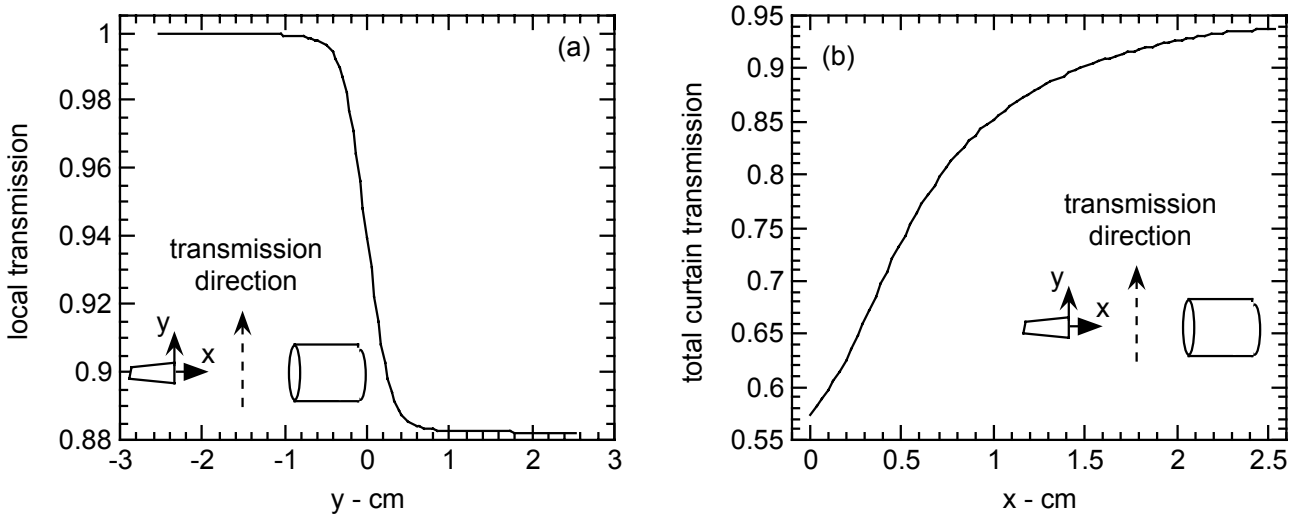

Figure 20. Calculated results for the EUV transmission through the curtain for a helium flow rate of 760 Tl/s. (a) The local transmission in the y-direction through the center of the curtain as a function of the y-coordinate. (b) The total transmission in the y-direction (through a 5 cm thick region surrounding the curtain) as a function of the x-coordinate.

Experimental confirmation of calculated results for particle trajectories using the data such as that in Figure 13 cannot be made because the velocity and size of the particles are not known. However, calculations can be used to infer some of the characteristics of the particles based on their trajectories. That is, through a trial and error process a combination of particle material, size and initial velocity can be found that gives a calculated trajectory that matches the experimental result. This is shown in Figure 21, where the calculated trajectory matches closely that seen in Figure 13. Based on this the particle may have been 17 g/cm^3 with a 1 micron diameter and an

initial speed of 35 m/s. Of course, the combination of particle size and speed that matches the measured trajectory is not unique, e.g. a particle diameter of 10 microns and an initial speed of 10 m/s would also give a trajectory close to that seen in Figure 13. With more detailed information on the particle size distribution, studies of advanced gas curtain designs can be carried out using a modeling approach.

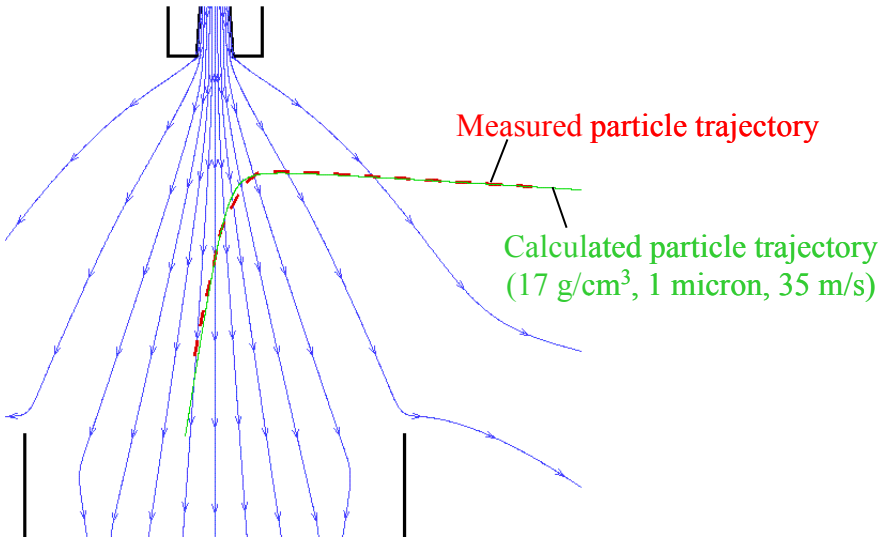

Figure 21. A comparison of measured and calculated particle trajectories. The calculated trajectory is for a 17 g/cm^3 particle with a diameter of 1 micron and an initial particle speed of 35 m/s.

6. Conclusions

Experiments and simulations were carried out to study the effectiveness of a gas curtain for mitigating debris generated by electric discharge light sources. A supersonic gas jet was used to form the curtain and a diffuser was used to capture and remove some of the gas in order to help maintain low pressures (and small EUV absorption losses) in the vacuum chamber. Large diffuser capture efficiencies were obtained in the experiments using high gas flow rates and the pressure in the vacuum chamber was maintained to acceptably low values. The helium gas curtain with a flow rate of 760 torr l/s resulted in a significant and unmistakable reduction in mirror erosion and particulate debris deposited on a witness plate. However, some debris was deposited on the witness plate with the gas curtain in operation, so further study is required to determine the path of this debris to the witness plate.

The calculations were validated (partially) by comparison with the measured results for the diffuser efficiency and a particle trajectory. Calculated results for the EUV transmission through the gas curtain showed it to be acceptable. Further study of gas curtain designs can be carried out using a modeling approach, although experimental study will continue to be required until a more complete understanding of the characteristics of the particulate debris is obtained. Issues that may be studied include curtain designs giving improved EUV transmission and designs that better contain the debris such that it cannot circumnavigate the curtain.

7. References

1. H.A. Bender, D. O'Connell and W.T. Silfvast, "Velocity characterization of particulate debris from laser-produced plasmas used for extreme-ultraviolet lithography", Center of Research and Education in Optics and Lasers, University of Central Florida, May, 1995.
2. C.B. Henderson, "Drag coefficients of spheres in continuum and rarefied flows", AIAA J., Vol. 14, pp. 707-708, 1976.

8. Distribution

1	MS 0513	Al Romig, 1000
1	MS 0619	Review & Approval Desk 12690
1	MS 9409	Bill Replogle, 8731
1	MS 9409	Glenn Kubiak, 8732
1	MS 9409	John Goldsmith, 8730
10	MS 9409	Neal Fornaciari, 8730
1	MS 9409	William P. Ballard, 8732
1	MS9409	Howard Bender, 8730
10	MS9042	Mike Kanouff, 8728
1	MS9402	Dean Buchenauer, 8724

3	MS 9018	Central Technical Files, 8945-1
1	MS 0899	Technical Library, 9616
1	MS 9021	Classification Office, 8511/Technical Library, MS 0899, 9616
1		DOE/OSTI via URL
1	MS 0188	D. Chavez, LDRD Office, 4001